Removal of pharmaceuticals in pre-denitrifying MBBR – Influence of organic substrate availability in single- and three-stage configurations

Fabio Polesel[1,*], Elena Torresi[1], Luca Loreggian[1,2], Monica Escolá Casas[3], Magnus Christensson[4], Kai Bester[3], Benedek Gy. Plósz[1,5,*]

[1]DTU Environment, Technical University of Denmark, Bygningstorvet B115, 2800 Kongens Lyngby, Denmark

[2]Environmental Engineering Institute, Ecole Polytechnique Fédérale de Lausanne, Station 6, 1015 Lausanne, Switzerland

[3]Department of Environmental Science, Aarhus University, Frederiksborgvej 399, 4000 Roskilde, Denmark

[4]Veolia Water Technologies AB, AnoxKaldnes, Klosterängsvägen 11A, SE-226 47 Lund, Sweden

[5]Department of Chemical Engineering, University of Bath, Claverton Down, Bath BA2 7AY, UK

Corresponding authors: fabp@env.dtu.dk, b.g.plosz@bath.ac.uk

Abstract

Due to the limited efficiency of conventional biological treatment, innovative solutions are being explored to improve the removal of trace organic chemicals in wastewater. Controlling biomass exposure to growth substrate represents an appealing option for process optimization, as substrate availability likely impacts microbial activity, hence organic trace chemical removal. This study investigated the elimination of pharmaceuticals in pre-denitrifying moving bed biofilm reactors (MBBRs), where biofilm exposure to different organic substrate loading and composition was controlled by reactor staging. A three-stage MBBR and a single-stage reference MBBR (with the same operating volume and filling ratio) were operated under continuous-flow conditions (18 months). Two sets of batch experiments (day 100 and 471) were performed to quantify and compare pharmaceutical removal and denitrification kinetics in the different MBBRs. Experimental results revealed the possible influence of retransformation (e.g., from conjugated metabolites) and enantioselectivity on the removal of selected pharmaceuticals. In the second set of experiments, specific trends in denitrification and biotransformation kinetics were observed, with highest and lowest rates/rate constants in the first (S1) and the last (S3) staged sub-reactors, respectively. These observations were confirmed by removal efficiency data obtained during continuous-flow operation, with limited removal (<10%) of recalcitrant pharmaceuticals and highest removal in S1 within the three-stage MBBR. Notably, biotransformation rate constants obtained for non-recalcitrant pharmaceuticals correlated with mean specific denitrification rates, maximum specific growth rates and observed growth yield values. Overall, these findings suggest that: (i) the long-term exposure to tiered substrate accessibility in the three-stage configuration shaped the denitrification and biotransformation capacity of biofilms, with significant reduction under substrate limitation; (ii) biotransformation of pharmaceuticals may have occurred as a result of cometabolism by heterotrophic denitrifying

bacteria.

Keywords: Moving bed biofilm reactors, pharmaceutical biodegradation, heterotrophic denitrification, reactor staging, organic substrate

1. Introduction

Elimination of pharmaceuticals and other trace organic chemicals represents a major challenge in conventional wastewater treatment systems. Innovative solutions, e.g., novel treatment technologies or process configurations, have been explored to improve the removal efficiency in biological wastewater treatment facilities.

Among the plethora of evaluated options, staging of biological reactors (defined as the subdivision into two or more completely mixed sub-reactors in series) has been proposed to optimize pollutant removal processes based on reaction kinetic principles (Scuras et al., 2001; Joss et al., 2006; Grady et al., 2011). Staging of pre-denitrifying reactors (Plósz, 2007; Plósz et al., 2010a) was accordingly hypothesized to enhance denitrification as compared to single-stage configurations. In staged systems with prolonged physical biomass retention (i.e. as biofilms), microbial adaptation to specific substrate availability conditions can be induced in each sub-stage. As to pre-denitrifying systems, shaping of microbial activity and community is determined by the availability and the quality (e.g., in terms of degradability) of electron donating organic substrate. Nevertheless, it is unknown how reactor staging would impact the removal (via biotransformation) of trace organic chemicals. Although it has been hypothesized that the degradation of more recalcitrant organics (such as xenobiotics) would occur in substrate-limited staged denitrifying reactors (Plósz et al., 2010a)—as also observed under aerobic conditions (Escolá Casas et al., 2015)—no evidence is currently available.

Recently, moving bed biofilm reactors (MBBRs) have been considered as an option to improve the removal of pharmaceuticals. In MBBRs, biomass grows on suspended plastic carriers (Ødegaard et al., 1994), with expected increase of biomass residence time compared to activated sludge systems. Enhanced biotransformation was accordingly observed in nitrifying MBBRs for a number of pharmaceuticals (Falås et al., 2012, 2013; Torresi et al., 2016). As the wide majority

74 of studies have focused on aerobic conditions (in line with overall literature on biodegradation
75 of xenobiotics; Ghattas et al., 2017), little is known about denitrifying MBBRs, with detailed
76 information only recently obtained for post-denitrifying systems (Torresi et al., 2017).
77 In this study, we investigated the elimination of pharmaceuticals in single-stage and three-stage
78 MBBR configurations for pre-denitrification of municipal wastewater. We assessed the effect of
79 organic substrate availability on pharmaceutical degradation and ensured prolonged biomass
80 exposure (via immobilization on carriers) to specific substrate availability conditions. During
81 long-term continuous operation of the two systems, batch experiments were performed at two
82 distinct time points to assess kinetics of heterotrophic denitrification and pharmaceutical
83 removal in each MBBR. Indigenous pharmaceutical concentrations in wastewater media were
84 used in the study, given the potentially significant influence of spiking on transformation kinetics
85 and pathways (Collado et al., 2012; Jewell et al., 2016) as well as the possibility of
86 retransformation from conjugated metabolites and structural analogues (Polesel et al., 2016).
87 The main objectives of our investigation were: (i) to assess and compare kinetics of
88 denitrification (primary metabolic function) and pharmaceutical biotransformation (secondary
89 metabolic function) in different MBBR systems; (ii) to assess the influence of biofilm exposure
90 to different organic substrate loading and complexity, resulting from MBBR staging, on its
91 capability of reducing nitrate and nitrite and biotransforming selected pharmaceuticals; and (iii)
92 to eventually investigate the association between primary and secondary metabolic functions.
93 Specifically, two alternative hypotheses were tested:
94 • Strongly limiting organic substrate availability (in the downstream reactor stages) induces an
95 improvement of pharmaceutical biotransformation kinetics, due to the possible improvement
96 in utilizing more recalcitrant chemicals (e.g. of pharmaceuticals) as secondary/secondary-
97 cometabolic substrates;

- Non-limiting organic substrate availability (occurring in the upstream reactor stages) positively influences pharmaceutical biotransformation kinetics by more effectively fueling denitrifying activity.

2. Materials and methods

2.1. System description and operation

Two laboratory scale pre-denitrifying MBBR configurations with K1 carriers (AnoxKaldnes, Lund, Sweden; specific surface area = 500 m^2 m^{-3}) were operated in parallel under continuous-flow conditions for 1.5 years (Fig. 1). The two configurations were operated under identical conditions, i.e. influent flow rate, hydraulic residence time, influent medium characteristics, to allow for a comparative assessment of system performance.

The single-stage configuration included a single bioreactor (U) with operating volume of 6 L. The three-stage configuration was designed according to principles presented by Plósz (2007) and included three reactors in series (named S1, S2, S3) with a total operating volume of 6 L (1.5 L for S1 and S2 and 3 L for S3). To limit O_2 penetration, reactors were continuously sparged with N_2 gas (≥ 99.996%, Aga A/S, Copenhagen, Denmark) and provided with polystyrene lids and rubber top sealing, having a small opening that allowed for sparging gas to escape. These solutions allowed establishing DO concentrations lower than 0.05 mg L^{-1} in all MBBRs for the duration of the experiment. Sparging of N_2 gas was also used for mechanical mixing of K1 carriers.

MBBR carriers with attached biofilm used for reactor seeding were collected from the post-denitrification zone of Sjölunda WWTP (Malmö, Sweden). The post-denitrifying train of Sjölunda WWTP consists of two tanks in series, whereby dosage of external carbon source (methanol) takes place in the first tank of the treatment train while MBBR carriers (and attached

122 biofilms) were collected from the second tank. A filling ratio of 33% was selected for all reactors.
123 All MBBRs were operated at ambient temperature (?).
124 The two configurations were continuously fed with primary wastewater effluent (Mølleåværket
125 WWTP, Lundtofte, Denmark) at an influent flow rate of 15 L d^{-1} for each system. Pre-clarified
126 wastewater was collected semi-weekly, stored in a 200 L stirred cooling tank (< 4°C) and fed to
127 the MBBR reactors using a peristaltic pump (Ole Dich, Hvidovre, Denmark). Nitrate was
128 supplied to both MBBR systems from a 10 g L^{-1} dosing solution of KNO_3 (≥ 99.9%, Merck
129 Millipore, Darmstadt, Germany), fed at a flow rate of 1.2 L d^{-1} using another peristaltic pump
130 (Ole Dich, Hvidovre, Denmark). The resulting influent nitrate concentration (103 mgN L^{-1})
131 ensured that there was a residual nitrate in the treated effluent, thereby allowing for
132 denitrification to occur in all of the reactors at all times, i.e. that MBBR biofilm could
133 permanently be subject to anoxic conditions. As in full-scale pre-denitrifying systems, the
134 indigenous COD content of pre-clarified wastewater was the only electron donor available for
135 denitrification, i.e. no extra carbon source was supplied. Furthermore, during the entire operation
136 period both systems received only indigenous pharmaceutical concentrations present in the
137 feeding medium.
138 The two MBBR systems were monitored during continuous-flow operation for approximately
139 1.5 months before and/or after batch experiments (see Chapter 2.2). System performance in terms
140 of heterotrophic denitrification and pharmaceutical removal was assessed by monitoring influent
141 and effluent concentrations of COD, NO_3-N, NO_2-N and pharmaceuticals (see section S4, Table
142 S5). Characterization of organic substrates in the influent wastewater was carried out according
143 to Roeleveld and van Loosdrecht (2002).
144 **< Figure 1 >**
145

146 ***2.2. Batch experiments***

147 *2.2.1. Biotic*

148 Batch experiments were performed to assess biokinetics of heterotrophic denitrification and
149 pharmaceuticals elimination in the four MBBRs (U, S1, S2, S3). Two sets of batch experiments
150 were performed during 1.5 year of continuous operation: Batch 1 (day 100) and Batch 2 (day
151 471). In both cases, the continuous MBBR systems were disconnected and experiments were
152 performed with carriers from U, S1, S2 and S3 separately at the same boundary and initial
153 conditions (feeding medium characteristics, filling ratio, reactor operation).

154 Similarly to continuous-flow operation, pre-clarified wastewater from Mølleåværket WWTP
155 was used as feeding medium in batch experiments. The medium was supplemented with KNO_3,
156 resulting in an initial NO_3-N concentration of 100–104 mgN L^{-1}. DO concentration was
157 minimized through continuous sparging of N_2 gas. Temperature and pH were continuously
158 monitored (SenTix® 980, WTW, Weilheim, Germany). Manual pH adjustment with 1 M HCl
159 was performed at the beginning and through the experiment to prevent microbial activity
160 inhibition. Experiments were performed at ambient temperature. Spiking of reference
161 pharmaceuticals was not used, and only the indigenous chemicals occurring in pre-clarified
162 wastewater were quantified. Aqueous samples for the analysis of pharmaceuticals and
163 conventional pollutants were withdrawn from MBBRs and concurrently a fixed number of
164 carriers were removed to maintain a constant filling ratio.

165 The duration of Batch 1 was 24 h, with MBBR filling adjusted to 20%. The temperature during
166 batch experiments was (mean and standard deviation, 5 min frequency): 20.3 ± 0.9°C for S1,
167 20.2 ± 1.3°C for S2, 20.3 ± 1.0°C for S3, 20.3 ± 0.9°C for U. In Batch 2, a filling ratio of 10%
168 was used and the experiment duration was extended to 49 h. The temperature during batch
169 experiments was (mean and standard deviation, 10 min frequency): 16.7 ± 0.5°C for S1, 17.4 ±

0.5°C for S2, 16.8 ± 0.4°C for S3, 17.0 ± 0.5°C for U.

2.2.2. Control experiments

A reference batch experiment (abiotic control experiment) was additionally performed to assess abiotic degradation of pharmaceuticals, based on the methodology proposed by Falås et al. (2013). The experiment was conducted in a glass container with 200 mL pre-filtered (GF filter, 0.6 µm pore size, Advantec, Knebel, Denmark) pre-clarified wastewater (Mølleåværket WWTP, Lundtofte, Denmark). Reactor mixing was ensured by N_2 gas sparging. The experiment was conducted in the absence (first 2 h) and in the presence of plastic carriers without biofilm (last 2 h), with an overall duration of 4 h. Aqueous samples were withdrawn at t=0, 2 and 4 h. An evaporation control experiment was additionally carried out in parallel to assess the evaporation of filtered wastewater due to N_2 gas sparging. Two glass containers (working volume = 200 mL) were operated in parallel and under the same conditions of the reference control experiment. Residual liquid volume was measured in the two reactors after 2 h and 4 h, respectively.

2.3. Analytical methods

Samples for the analysis of conventional pollutants were collected and analysed for total and soluble COD, NO_3-N and NO_2-N. Non-filtered and filtered samples (0.45 µm GF filters; Sartorius, Göttingen, Germany) were stored in plastic vials at ≤ 4°C until analysis (for non-filtered samples, within 24 h from collection). COD concentrations were quantified using Hach-Lange colorimetric kits (LCK314, LCK514) and Hach-Lange DR 2800 spectrophotometer. NO_3-N and NO_2-N concentrations were quantified with Merck colorimetric kits and subsequent spectrophotometric quantification (batch 1) or with a Bran Luebbe® Auto Analyzer 3 digital colorimeter (batch 2).

194 The concentration of attached biomass was determined from the weight difference of multiple
195 (≥ 5) dried carriers (105°C for >1 h) before and after biofilm removal, as described in Falås et
196 al. (2012). Attached biofilm was removed from plastic carriers using H_2SO_4 (4M) and thorough
197 brushing. The resulting biomass concentration was expressed in terms of total attached solids
198 (gTAS L^{-1}). Conversion factors TSS/TAS and VSS/TAS for biofilm in each MBBR were
199 determined via parallel measurements of TAS, TSS and VSS content. Biofilm from five carriers
200 for each MBBR was detached and resuspended in 50 mL tap water. Four replicate measurements
201 were performed, with overall biofilm detachment from 20 carriers per MBBR. TAS (in analogy
202 with total solids), TSS and VSS concentrations of the suspension were measured according to
203 APHA standard methods (Clesceri et al., 1998). Determination of TSS/TAS ratio allowed
204 converting attached biomass concentration to gTSS L^{-1}. The overall TSS concentration in each
205 MBBR was eventually determined by accounting for TSS in bulk aqueous phase (separate
206 measurement according to APHA standard methods).
207 Samples for pharmaceutical analysis were collected and prepared according to the procedure
208 described by Escolá Casas et al. (2015). Briefly, 4 ml wastewater samples were collected and
209 stored in glass vials (Chromacol 22 mL, Mikrolab, Aarhus, Denmark). 1.4 ml pure methanol (≥
210 99.9%, Merck Millipore) was added to inhibit biological activity during the storage period.
211 Prepared samples were then preserved at -20°C. Subsequently, 1.5 mL was of each sample were
212 transferred to an HPLC vial and were centrifuged (6000 rpm, 10 minutes) to separate residual
213 solids. 900 µL of the supernatant were transferred to a new vial, to which 100 µL of internal
214 standard solution were added using a glass syringe. Samples were analyzed using HPLC-MS/MS
215 with an injected volume of 100 µL. Twenty-three active pharmaceutical substances, typically
216 present in wastewater influents, were targeted. A complete list of these substances is given in
217 the Supporting Information (section S4) and elsewhere (Escolá Casas et al., 2015).

Specifications of the HPLC-MS/MS analytical device and of the internal standard solution can be found in Escolá Casas et al. (2015).

2.4. Anoxic respirometry

In batch 1 and 2, heterotrophic denitrification was assessed by measuring NO_3-N and NO_2-N (mgN L^{-1}) concentrations in different MBBRs. NO_2-N concentration was measured due to the possibility of nitrite accumulation, as shown in previous experiments (Ubay Çokgör et al., 1998; Kujawa and Klapwijk, 1999; Ekama and Wentzel, 1999), thus being accounted for when characterizing denitrification kinetics. Based on measured NO_3-N and NO_2-N concentrations, anoxic respirograms were derived for each batch experiment as NO_X utilization curves, where NO_X-N concentration (mgN L^{-1}) was calculated according to Eq. 1 (Ubay Çokgör et al., 1998):

$$NO_X - N = NO_3 - N + 0.6NO_2 - N \quad (1)$$

In this equation, the coefficient 0.6 denotes the relative amount of electrons required to reduce NO_2 to N_2 (3 e^-) compared to the reduction of NO_3 to N_2 (5 e^-). It is anticipated that two distinct NO_X utilization rates could be distinguished during batch experiments (Fig. S5). Fast slow specific denitrification rates (k_1 and k_2, respectively; mgN $gTSS^{-1}$ d^{-1}) were accordingly derived in each MBBR through linear regression of NO_X concentrations and normalization to biomass concentration (as gTSS L^{-1}). In order to provide for a unique kinetic descriptor of denitrification, the mean specific denitrification rate $\bar{k}_{NOX}$ (mgN $gTSS^{-1}$ d^{-1}) was calculated (Eq. 2):

$$\bar{k}_{NOX} = \frac{k_1 + k_2}{2} \quad (2)$$

Surface-normalized mean denitrification rates ($\bar{r}_{NOX}$, r_1 and r_2, gN m^{-2} d^{-1}) were also derived for each MBBR. The rationale for the interpretation of anoxic respirometric data, as well as the definition of denitrification rates, is described in detailed in the Supporting Information (section

241 S3).

242

243 ***2.5. Modelling pharmaceutical removal kinetics***

244 Based on observations on pharmaceutical removal in Batch 1 and 2, model structures were
245 identified using the Activated Sludge Model framework for Xenobiotics (ASM-X) (Plósz et al.,
246 2010b, 2012), including recent extensions presented by Torresi et al. (2017). A summary of
247 identified model structures is shown in Table 1.

248 In the simplest model structure, pseudo-first-order degradation kinetics was used to describe
249 aqueous concentration decrease (Eq. 3)

250 $$\frac{dC_{LI}}{dt} = -\frac{k_{bio}}{(1+K_d X_{TSS})} C_{LI} X_{TSS} \quad (3)$$

251 where C_{LI} denotes the aqueous pharmaceutical concentration (ng L^{-1}), k_{bio} the biotransformation
252 rate constant (L $gTSS^{-1}$ d^{-1}) and X_{TSS} the biomass concentration in MBBRs (gTSS L^{-1}). A
253 correction factor for sorption was considered, where K_d (L g^{-1}) denotes the sorption coefficient,
254 assuming instantaneous equilibrium between aqueous and sorbed concentrations (Joss et al.,
255 2006). Constant X_{TSS} was assumed, considering negligible biomass growth during batch
256 experiments. The effect of diffusion into biofilm on the removal of pharmaceuticals from bulk
257 aqueous phase was lumped in the biotransformation rate constants (Falås et al., 2012, 2013;
258 Escolá Casas et al., 2015; Torresi et al., 2016, 2017).

259 The transformation of human metabolites and other fractions (Polesel et al., 2016) may lead to
260 the formation of parent compounds and can be additionally described using pseudo-first-order
261 kinetics (Eq. 4):

262 $$\frac{dC_{CJ}}{dt} = -k_{dec} C_{CJ} X_{TSS} \quad (4)$$

263 where the state variable C_{CJ} denotes the retransformable pharmaceutical fractions (e.g.,

conjugated metabolites) and k_{dec} (L $gTSS^{-1}$ d^{-1}) denotes the retransformation rate constant. Negligible sorption was considered for the fraction C_{CJ} due to its potentially high hydrophilicity (Göbel et al., 2005; Plósz et al., 2010b). Simultaneous parent compound formation and biotransformation were thus described using Eq. 5:

$$\frac{dC_{LI}}{dt} = -\frac{k_{bio}}{(1+K_d X_{TSS})} C_{LI} X_{TSS} + k_{dec} C_{CJ} X_{TSS} \quad (5)$$

or, in case of only one major conjugated metabolite, using Eq. 6:

$$\frac{dC_{LI}}{dt} = -\frac{k_{bio}}{(1+K_d X_{TSS})} C_{LI} X_{TSS} + \frac{M_{LI}}{M_{CJ}} k_{dec} C_{CJ} X_{TSS} \quad (6)$$

where M_{LI} and M_{CJ} (g mol^{-1}) denote the molecular mass of the parent compound and the conjugate, respectively, and their ratio denotes the stoichiometry coefficient of retransformation (Plósz et al., 2013; Torresi et al., 2017).

2.6. Parameter estimation

Estimation of transformation rate constants (k_{bio}, k_{dec}) required the initial assumption of K_d. Values measured in activated sludge—where available under denitrifying conditions—were collected from published literature (Ternes et al., 2004; Göbel et al., 2005; Maurer et al., 2007; Radjenovic et al., 2009; Wick et al., 2009; Plósz et al., 2010b; Hörsing et al., 2011; Plósz et al., 2012). In absence of published K_d values, negligible sorption was assumed. Table S6 summarizes K_d values for detected pharmaceuticals.

When parent compound formation was observed in the absence of C_{CJ} measurements, the initial concentration $C_{CJ,0}$ (ng L^{-1}) was defined by assuming the same initial ratio $n_{LI,CJ}$ (Eq. 7) in all simultaneous batch experiments:

$$n_{LI,CJ} = \frac{C_{LI,0}}{C_{CJ,0}} \quad (7)$$

where $C_{LI,0}$ denotes the initial parent compound concentration (ng L^{-1}). In this case, calibration of Eq. 5 was performed for all experiments simultaneous, also with the estimation of $n_{LI,CJ}$. In all cases, model calibration against experimental data in Batch 1 and 2 was performed using the secant method embedded in Aquasim 2.1d (Reichert, 1998). Surface-normalized transformation rate constants (L^{-1} m^{-2} d^{-1}) were eventually calculated from estimated k_{bio} and k_{dec} values.

< Table 1 >

3. Results and discussion

3.1. Heterotrophic denitrification

3.1.1. Monitoring during continuous-flow operation

Due to considerable fluctuations in the quality of the wastewater influent, dynamics in NO_X removal were shown (Table S1, Fig. S2). Variability was observed in terms of influent concentrations of total COD (207 ± 57.3 mgCOD L^{-1}), soluble COD (84 ± 25.7 mgCOD L^{-1}), biodegradable COD (136 ± 41.6 mgCOD L^{-1}), readily biodegradable COD (S_S, 60.5 ± 25.0 mgCOD L^{-1}) and hydrolizable COD (X_S, 75.4 ± 36.5 mgCOD L^{-1}). NO_X removal per influent total COD was calculated, being 0.15–0.18 mgNO_X-N $mgCOD^{-1}$ for three-stage MBBR and 0.12–0.16 mgNO_X-N $mgCOD^{-1}$ for single-stage MBBR (Table S2). NO_2-N accumulation in the MBBR reactors was accounted for when calculating NO_X removal as shown in Eq. 1.

Surface-normalized NO_X removal rates exhibited a significant decrease after 400 days of operation (Table S2). This may be attributed to the reduced average influent loading of organic substrate (before day 100: 3.95 ± 0.87 gCOD d^{-1}; after day 400: 2.66 ± 0.41 gCOD d^{-1}; here expressed as total COD).

Reactor staging effectively determined a declining gradient of influent substrate loading from S1 to S3 (Table S3). Temporal trends of attached biomass concentration (gTAS L^{-1}) in each MBBR indicated significant growth as compared to the inoculum (Fig. S1). Faster growth was observed in S1, with stable biomass concentration reached after approximately 80 days, as compared to the other reactors (> 100 d). Towards the end of the operation period, the highest biomass concentration was found in S2 (5.2 gTAS L^{-1}) and comparable concentrations were found in the other MBBRs (3.9–4.2 gTAS L^{-1}).

3.1.2. Batch experiments (1 and 2)

317 Measured concentration profiles of NO_3-N, NO_2-N, total and soluble COD are presented in Fig.
318 S3 (Batch 1) and Fig. S4 (Batch 2). In all experiments, NO_2-N accumulation was observed, being
319 more prominent in batch 2 (up to 10 mgN L^{-1} in S3). The residual soluble COD concentration
320 was found comparable (52.7 ± 3.2 mgCOD L^{-1} in batch 1; 53.9 ± 6.9 in batch 2), representing
321 the inert organic matter not utilizable as electron donor.
322 In batch 1, depletion of organic substrate in the wastewater medium (based on soluble COD
323 measurements) was reached after 0.2–0.4 d, typically coinciding (except for S3) with a change
324 in NO_X reduction rate (Fig. S5a). As to NO_X reduction kinetics, no trend was shown for $\bar{k}_{NOX}$ in
325 the three staged MBBRs (Table S4).
326 A number of peculiar observations were made during batch 2, which will be thus discussed more
327 in detail. Fig. 2 presents measured concentration profiles of NO_X (a) and total COD (b) in the
328 different MBBRs during batch 2. Experimental data revealed significantly different
329 denitrification capacity and kinetics in MBBRs. Notably, initial lag phases in NO_X reduction
330 were found in S2, U (1.5 h) and S3 (3 h) (Fig. 2a), possibly resulting from the prior limited
331 exposure of biofilm in these MBBRs to readily biodegradable organic substrate. As to S2 and
332 S3, this indicates that the three-staged reactor design achieved exposing biofilm to limiting and
333 highly limiting organic substrate, respectively (Plósz, 2007). Furthermore, NO_X reduction during
334 continuous-flow operation predominantly relied on hydrolysis products also in the single-stage
335 system U.
336 NO_X reduction rates were determined by neglecting the initial lag phase (Fig. S5). Calculated
337 $\bar{k}_{NOX}$ values were 48.2 mgN $gTSS^{-1}$ for S1, 18.9 mgN $gTSS^{-1}$ for S2, 12.4 mgN $gTSS^{-1}$ for S3
338 and 20.3 mgN $gTSS^{-1}$ for U. When considering the three-stage system, $\bar{k}_{NOX}$ (and the surface-
339 normalized rate $\bar{r}_{NOX}$) declined from S1 to S3, indicating that different organic substrate loading
340 and availability influenced both the capacity and the kinetics of NO_X reduction in MBBR

biofilm. A substantial decrease of $\bar{k}_{NOX}$ and $\bar{r}_{NOX}$ was observed in batch 2 as compared to batch 1 (Table S4), being more pronounced in S2, S3 and U. Not unexpectedly, both biomass- and surface-normalized rates were significantly lower than in post-denitrifying MBBRs, where only easily degradable external organic substrate is used as electron donor (Torresi et al., 2017).

Different levels of NO_X reduction were achieved in all MBBRs with comparable total COD removal (ΔCOD=257–275 mgCOD L^{-1} over 48 h) and utilization kinetics (Fig. 2b). Accordingly, COD storage may have occurred in S2, S3 and U due to biofilm exposure to feast substrate availability conditions following prolonged famine during continuous-flow operation, as previously shown for denitrifying bacteria (Beun et al., 2000). The microbial growth yield, Y_H (mgCOD $mgCOD^{-1}$) was thus calculated based on measured NO_X and COD concentrations. The calculation of Y_H (Eq. 8) was based on NO_X and COD utilization during fast denitrification (without considering the initial lag phase in S2, S3 and U), thus better approximating the true yield:

$$Y_H = 1 - \frac{2.86 \cdot \Delta NO_X}{\Delta COD} \quad (8)$$

where 2.86 (mgCOD mgN^{-1}) denotes the COD equivalents of NO_X-N (with the reduced number of COD equivalents of NO_2-N accounted for in Eq. 1). ΔNO_X (mgN L^{-1}) and ΔCOD (mgCOD L^{-1}) denote the NO_X and total COD utilized during fast denitrification in batch 2, respectively, and were quantified using an intercept-based method. Further details on the method (and examples for S1 and S3) are provided in Fig. S6. A value of 0.53 was calculated for Y_H in S1, in agreement with typical values for denitrification (Ubay Çokgör et al., 1998). Higher Y_H values were instead found for S2, S3 and U (0.61, 0.77 and 0.67, respectively), further suggesting the occurrence of substrate storage in these MBBRs (Muller et al., 2003).

Furthermore, maximum specific growth rates (μ_{max}) in each MBBR were derived from the fast

364 denitrification rate k_1 (using the calculated yield Y_H), according to the method proposed by
365 Ekama and Wentzel (2008). Estimated μ_{max} values were 0.22, 0.12, 0.16 and 0.17 d^{-1} in S1, S2,
366 S3 and U, respectively. These values were lower than that estimated for nitrate and nitrite
367 reduction in activated sludge using single organic substrate (Pan et al., 2015), but were in
368 agreement with estimations for ethanol-fed post-denitrifying MBBR (Torresi et al., 2017). It
369 should be noted that the presented values may include (for S2, U and especially S3) both the
370 rates of growth and simultaneous substrate storage.

371 **< Figure 2 >**

372

373 **3.2. Removal of pharmaceuticals**

374 Based on measured concentrations during continuous-flow operation and in batch 1 and 2, it was
375 possible to characterize the removal of a number of substances, namely: (i) the beta-blockers
376 atenolol (ATN) and metoprolol (MET); (ii) the sulfonamide antibiotics sulfamethoxazole
377 (SMX), sulfamethizole (SMZ), sulfadiazine (SDZ) and its conjugated metabolite acetyl-
378 sulfadiazine (AcSDZ), and the combination product trimethoprim (TMP); the macrolides
379 antibiotic erythromycin (ERY); (iv) the anti-inflammatory pharmaceuticals diclofenac (DCF)
380 and ibuprofen (IBU); (v) the X-ray contrast medium iohexol (IOH); (vi) and the anti-depressants
381 citalopram (CIT) and venlafaxine (VFX). Since only indigenous concentrations were considered
382 (i.e., no spiking of reference substances was performed), this is only a sub-sample of the initially
383 targeted pharmaceuticals. Further details on the quantified chemicals can be found in Table S5.
384 In the following sections, results will be thus presented and discussed for the listed substances.

385

386 *3.2.1. Abiotic transformation during control experiments*

387 Negligible (≤15%) or no removal was observed in the abiotic control experiment (Fig. S11), in
388 agreement with previous studies (Falås et al., 2012, 2013; Torresi et al., 2016). For almost all

389 substances (ATN, DCF, IOH, IBU, MET, SMZ, SDZ, AcSDZ, TMP, VFX), an increase of
390 aqueous concentration (on average +16%) was observed and could be attributed to wastewater
391 evaporation during the evaporation control experiment (Fig. S12).
392
393 *3.2.2. Biotransformation kinetics (batch 1 and 2)*
394 Measured pharmaceutical concentrations in batch 1 and 2 exhibited a number of typical patterns
395 (Fig. 3), which could be interpreted in most cases using Eq. 3–6. A complete overview of
396 measured concentration profiles in both batch experiments is given in Fig. S7–8. Differently
397 from NO_X reduction, no lag phase in the removal of pharmaceuticals was shown in batch 2.
398 Several pharmaceuticals (TMP in batch 1; ATN, ERY, IBU, IOH, SMZ, TMP and VFX in batch
399 2) exhibited elimination as in Figure 3a, following pseudo-first-order kinetics (Eq. 3) that were
400 described by k_{bio}.
401 Initial increase of aqueous concentration was observed for SMX, SDZ, DCF and MET (Fig. 3b–
402 c). Retransformation of these pharmaceuticals can occur from conjugated metabolites, structural
403 analogues and/or parent pharmaceuticals (Polesel et al., 2016) and was considered to explain
404 these profiles. SMX is excreted in the form of parent and two major conjugated metabolites, N_4-
405 acetyl-SMX and SMX-N_1-glucuronide (Vree et al., 1995; van der Ven et al., 1995), which were
406 shown to transform back to parent SMX in laboratory- and full-scale studies (Göbel et al., 2005;
407 Plósz et al., 2010; Radke et al., 2009; Stadler et al., 2015). SDZ is known to have only one major
408 conjugated metabolite, AcSDZ (Vree and Hekster, 1987), which could also be quantified during
409 batch 1 (Fig S6e–f). Eq. 4 and 6 were thus simultaneously calibrated to AcSDZ and SDZ
410 measurements, respectively, allowing for the estimation of k_{dec} and k_{bio}. DCF is also excreted as
411 sulfate and glucuronide conjugates (Stierlin and Faigle, 1979), and its formation was reported in
412 laboratory experiments (Lee et al., 2012) and in full-scale WWTPs (Zhang et al., 2008; Plósz et

al., 2012; Vieno and Sillanpää, 2014). As to MET, excretion as conjugated metabolite is negligible (Escher et al., 2006). Formation of MET was still observed in pilot- and full-scale WWTPs (Bendz et al., 2005; Radjenovic et al., 2009; Wick et al., 2009; de Graaff et al., 2011; Jelic et al., 2011). Although these observations have been attributed to sampling and/or analytical uncertainties (Alder et al., 2010), formation from a structurally analogue chemical may not be excluded (in particular under denitrifying conditions).

In two cases (ATN in batch 1, CIT in batch 2), Eq. 3 did not adequately describe batch removal kinetics. Notably, ATN and CIT are chiral and both enantiomers are present in wastewater (Kasprzyk-Hordern and Baker, 2011; Evans et al., 2015). Similar observations were made for another chiral pharmaceutical, propranolol (Escolá Casas et al., 2015). In analogy with the latter study, enantioselective biotransformation was hypothesized to determine the two-rate profile observed in batch experiments in all four MBBRs (Fig. 3d). Pseudo-first-order transformation kinetics was assumed for the two enantiomers, being described by rate constants $k_{bio,1}$ and $k_{bio,2}$ (L $gTSS^{-1}$ d^{-1}). Biotransformation of ATN and CIT was thus described according to Eq. 9 (Table 1):

$$\frac{dC_{LI}}{dt} = -\frac{1}{(1+K_d X_{TSS})}(k_{bio,1}C_{EN,1} + k_{bio,2}C_{EN,2})X_{TSS} \quad (9)$$

where $C_{EN,1}$ and $C_{EN,2}$ (ng L^{-1}) denote the aqueous concentrations of the two enantiomers, respectively, and C_{LI} (ng L^{-1}) is the sum of $C_{EN,1}$ and $C_{EN,2}$. Initial conditions for $C_{EN,1}$ and $C_{EN,2}$ were set by considering in all simultaneous batch experiments the same initial enantiomeric fraction *EF* (Ribeiro et al., 2013; Eq. 10):

$$EF = \frac{C_{EN,1}(t=0)}{C_{EN,1}(t=0)+C_{EN,2}(t=0)} = \frac{C_{EN,1}(t=0)}{C_{LI}(t=0)} \quad (10)$$

Through calibration of Eq. 9 to all batch experiments simultaneously, the parameters $k_{bio,1}$, $k_{bio,2}$

435 and EF could be estimated. The enantioselective biotransformation model (Fig. 3d; Fig. S7a and
436 S8k) was shown to significantly improve the prediction of measured concentrations for ATN
437 and CIT (R^2 = 0.95–0.99) as compared to a simple first-order equation (Fig. S9). Nevertheless,
438 this hypothesis requires further confirmation, with identification and quantification of the two
439 enantiomers of ATN and CIT.

440 **< Figure 3 >**

441 Estimated rate constants (k_{bio}, k_{dec}, $k_{bio,1}$, $k_{bio,2}$) in batch 1 and 2 are presented in Fig. 4 (a and b,
442 respectively). In Table 2, rate constants from this study are compared with literature values for
443 denitrifying activated sludge (DNAS), nitrifying MBBR (NMBBR) and post-denitrifying MBBR
444 (DNMBBR).

445 In batch 1, the highest rate constant values were estimated either for S1 or U (Fig. 4a), while no
446 overall trend could be identified when considering staged MBBRs only. All the quantifiable
447 pharmaceuticals exhibited comparably high transformation and formation kinetics with the
448 exception of DCF. Rapid retransformation was shown, with k_{dec} typically higher than 1 L g^{-1}
449 TSS^{-1} and in agreement with previously observed formation (e.g., via deconjugation) kinetics
450 for diclofenac and sulfonamide antibiotics in activated sludge (Plósz et al., 2010b, 2012; Falås
451 et al., 2013) and MBBRs (Falås et al., 2013; Torresi et al., 2016, 2017).

452 In batch 2, the highest transformation rate constants were observed in S1 for all non-recalcitrant
453 pharmaceuticals (exhibiting k_{bio}, $k_{dec} \geq 0.1$ L $gTSS^{-1}$ d^{-1}, according to the classification presented
454 in Joss et al., 2006), with the exception of ATN. An overall decrease of the biotransformation
455 kinetics in U was shown compared to batch 1. Notably, the order of rate constant values in staged
456 MBBRs was consistently found to be S1>S2>S3 for all non-recalcitrant compounds, following
457 the gradient of (i) denitrification rates $\bar{k}_{NOX}$ observed in the same batch; and (ii) loading and
458 complexity of available organic substrate during continuous-flow operation. Given that all

459 MBBRs had the same specific surface area, the same consideration was valid for surface-
460 normalized biotransformation rate constants (Fig. S10).
461 In analogy with our study, decreasing influent COD loading was found to negatively influence
462 the removal efficiency of the estrogen E1 under aerobic conditions (Tan et al., 2013). The
463 relationship between pharmaceutical transformation and heterotrophic denitrification kinetics
464 will be discussed more in detail in section 3.3.
465 **< Figure 4 >**
466 Enhanced biotransformation kinetics, as compared to previous findings in DNAS were shown
467 for SMX, ATN and ERY (Table 2). In particular, k_{bio} values higher than 1.0 L $gTSS^{-1}$ d^{-1} were
468 found in S1, thus indicating a significant increase in biotransformation kinetics for MBBR
469 biofilm growing under non-limiting COD loading. Comparably high transformation kinetics was
470 also shown for SMX and ATN in DNMBBR, in the presence of methanol or ethanol was as
471 electron donor (Torresi et al., 2017). Nevertheless, significant differences in the transformation
472 kinetics of other substances (e.g., MET, SMZ and TMP) could be observed between pre- and
473 post-denitrifying conditions. This indicates that the type of electron donor used for NO_X
474 reduction influences not only the activity and the community composition of denitrifiers, but
475 also their capacity of biotransforming pharmaceuticals (including structural analogues, e.g. ATN
476 and MET).
477 Parent-to-retransformable chemical ratios in pre-clarified wastewater ($n_{LI,CJ}$) were estimated for
478 SMX, DCF and MET, indicating (particularly for SMX) comparably high concentration levels
479 of retransformable fractions (C_{CJ}). Values of $n_{LI,CJ}$ for SMX were in agreement with ratios
480 measured in pre-clarified sewage (Göbel et al., 2007; Plósz et al., 2010b).
481 Overall, DCF was found to be recalcitrant, in agreement with previous evidences from DNAS
482 and DNMBBR, but opposed to what observed in NMBBR (Table 2). In batch 2, other

483 pharmaceuticals (IBU, IOH, SMZ and VFX) were also found recalcitrant. IBU is known to be
484 rapidly biodegradable in activated sludge under aerobic conditions (k_{bio}>10 L $gTSS^{-1}$ d^{-1}; Joss et
485 al., 2006).While this has been observed also in NMBBRs (Escolá Casas et al., 2015; Torresi et
486 al., 2016), significant variability in rate constants was shown, whereby also negligible IBU
487 removal was reported (Falås et al., 2012). Reduced biotransformation was also found in DNAS
488 (Suarez et al., 2010) and DNMBBR (Torresi et al., 2017) as compared to aerobic conditions, still
489 significantly higher than in this study. In agreement with our findings, VFX underwent limited
490 degradation both in NMBBR and DNAS (Falås et al., 2013; Escolá Casas et al., 2015; Torresi et
491 al., 2016), while enhanced biotransformation via cometabolism was observed in the presence of
492 methanol or ethanol in DNMBBR (Torresi et al., 2017).
493 A number of differences were found between the two batch experiments. Values of k_{bio} for TMP
494 and MET significantly decreased in batch 2, still within the variability of literature rate constants
495 in DNAS and NMBBR (Table 2). Furthermore, tentative results supporting enantioselective
496 ATN biotransformation were found in batch 1. Assuming that both ATN enantiomers were
497 present also during batch 2, this may indicate limited enantioselectivity by MBBR biofilm as a
498 result of long-term adaptation. Preferential elimination of the S(-)-enantiomer of ATN was
499 reported in full-activated sludge WWTPs, whereas limited enantioselectivity was shown in
500 biofilm systems (e.g., trickling filters) (Kasprzyk-Hordern and Baker, 2011). Enantioselective
501 removal of CIT was also considered to explain *EF* variations between WWTP influent and
502 effluent (MacLeod et al., 2007; Evans et al., 2015). Measured *EF* ratios in WWTP influents were
503 similar to what estimated in this study for CIT, while differences were shown for ATN (Table
504 2).
505 **< Table 2 >**
506

507 *3.2.3. Removal efficiency during continuous-flow operation*

508 The removal of pharmaceuticals was also investigated during continuous-flow operation of the
509 single- and three-stage MBBRs, in proximity of batch 1 and 2. Removal efficiencies in the two
510 systems, calculated from influent and effluent concentrations, are shown in Table S7. Removal
511 efficiencies in each reactor stage (S1, S2 and S3) were calculated for ATN, CIT, TMP and ERY
512 (Fig. S14).

513 Generally, removal efficiencies were in agreement with observations from batch experiments.
514 ATN and CIT underwent relatively high removal in both single- and three-stage MBRRs (≥ 72%
515 and 56–67% respectively), as previously observed in post-denitrifying MBBR (HRT=2 h;
516 Torresi et al., 2017). Intermediate removal efficiencies (25–50%) were shown for TMP and ERY,
517 also similarly to ethanol- and methanol-dosed post-denitrifying MBBRs, respectively (Torresi
518 et al., 2017). Formation of SMX and DCF was shown, thus resulting in negative removal
519 efficiencies (up to -157%) that are in agreement with findings in full-scale WWTPs (Plósz et al.,
520 2010b, 2012; Göbel et al., 2005, 2007). Substances classified as recalcitrant based on estimated
521 k_{bio} also exhibited limited elimination (removal efficiency <10%).

522 In the three-stage system, non-recalcitrant and non-retransformable compounds showed highest
523 removal efficiency in S1 (Fig. S14) with the exception of TMP, which underwent the highest
524 removal in S3. Interestingly, differences between batch 1 and 2 were reflected by changes in
525 removal efficiency. SMX and TMP underwent increased (batch 1: -157% and -135%; batch 2: -
526 58% and -39%) and decreased (batch 1: 39% and 49%; batch 2: 24% and 29%) removal
527 efficiency, respectively, in line with changes in estimated k_{bio} values.

528

529 **3.3. Linking denitrification and pharmaceutical biotransformation (batch 2)**

530 Long-term system operation (>450 d) was instrumental in ensuring sufficient biomass adaptation

531 (Weiss and Reemtsma, 2008), as exemplified by differences between batch 1 and 2. Prolonged
532 exposure to increased organic substrate loading and availability in S1 corresponded to an
533 enhancement of denitrification and biotransformation kinetics. At the same time, biofilm in S1
534 had access to a broader and more diverse array of carbon sources (including pharmaceuticals),
535 likely including a higher fraction of readily degradable organic substrates. Hence, on the one
536 hand, a more active denitrifying community likely populated the biofilm in S1 compared to S3,
537 of which the latter included a higher fraction of inert biomass (Boltz et al., 2017). This may have
538 led to a positive influence on the cometabolic biotransformation of a number of pharmaceuticals
539 (as further discussed in this paragraph) in S1. On the other hand, the exposure to different organic
540 loading resulted in the development of microbial communities with different degree of
541 biodiversity in the three-staged MBBR, possibly influencing pharmaceutical biotransformation.
542 Preliminary results on the influence of reactor staging on microbial community composition in
543 the MBBRs can be found in Torresi (2017).
544 Findings in this study are in analogy with observations in a two-stage managed aquifer recharge
545 system, where carbon availability positively influenced the removal of a number of
546 pharmaceuticals (as well as denitrifying activity) under anoxic conditions (Hellauer et al., 2017).
547 Furthermore, increased carbon loading to aerobic activated sludge reactors was beneficial for
548 the removal of estrone (Tan et al., 2013). On the contrary, staging of aerobic MBBRs resulted
549 in an overall enhancement of biotransformation kinetics by substrate-limited biofilms in the last
550 reactor stage (Escolá Casas et al., 2015).
551 The relationship between denitrification and biotransformation kinetics in S1, S2, S3 and U was
552 further assessed in detail. Figure 5a and S12a present transformation rate constants for all non-
553 recalcitrant pharmaceuticals, i.e. SMX, ERY, TMP, ATN, and CIT, plotted as a function of $\overline{k}_{NOX}$
554 . Strong linear correlations were shown for SMX, ERY and TMP (R^2=0.90–0.99; Fig. 5a), while

555 weaker correlation was found for ATN and CIT (R^2=0.44–0.53; Fig. S13a). Interestingly,
556 varying regression slopes were shown for the selected pharmaceuticals, possibly indicating
557 significantly different transformation potential by denitrifying communities (independently of
558 the available organic substrate). Linear correlations have been previously observed between k_{bio}
559 and specific nitrification rates for several pharmaceuticals, including trimethoprim (Fernandez-
560 Fontaina et al., 2012).
561 Similarly, linear correlations were observed between k_{bio}, k_{dec} and μ_{max} (Fig. 5b) and 1-Y_H (Fig.
562 5c), although less strong as compared to $\bar{k}_{NOX}$ (R^2=0.54–0.78). The correlation obtained with
563 μ_{max} supports reasonably well the positive relationship between kinetics of denitrification and
564 pharmaceutical biotransformation. The parameter 1-Y_H denotes the fraction of electron
565 equivalents used for catabolic respiration (thus, NO_X reduction). Accordingly, the utilization of
566 organic substrate for storage and/or anabolism negatively influenced the removal of
567 pharmaceuticals, thus further suggesting the association biotransformation with denitrifying
568 activity. Taken together, these observations point towards the conclusion that biotransformation
569 of non-recalcitrant pharmaceuticals resulted from cometabolism by denitrifying bacteria.
570 Simultaneous increased loading and availability of organic substrate, as induced in reactor S1,
571 can result in a significant enhancement of both heterotrophic denitrification and pharmaceutical
572 biotransformation capacity as compared to single-stage systems and reactors operated under
573 substrate-limited conditions.
574 Considering the positive dependency with heterotrophic denitrification, a cometabolic
575 biotransformation model was proposed based on the correlations in Fig. 5a (Eq. 10):

576 $$\frac{dC_{LI}}{dt} = T_{C,NOX}\bar{k}_{NOX}C_{LI} \quad (10)$$

577 The coefficient $T_{C,NOX}$ (L mgN^{-1}; Eq. 11):

578 $$T_{C,NOX} = \frac{k_{bio,dec}}{\bar{k}_{NOX}} \quad (11)$$

579 is defined as the transformation coefficient associated to denitrification, and quantifies the
580 relative pharmaceutical mass (-) transformed per mgN L^{-1} reduced. $T_{C,NOX}$ was defined in analogy
581 to coefficients relating kinetics of pharmaceutical transformation and of ammonia oxidation
582 (Sathyamoorthy et al., 2013). Interestingly, selected pharmaceuticals exhibited a wide range of
583 $T_{C,NOX}$ values (0.005–0.072 L mgN^{-1}), indicating significantly different transformation potential
584 by denitrifying communities (independently of the available organic substrate). The presented
585 model represents one of the first attempts to describe cometabolic biodegradation under pre-
586 denitrifying conditions, and can be used for forward predictions of pharmaceutical removal as a
587 function of denitrifying activity. Nevertheless, this approach requires further confirmation
588 through validation with independent datasets.

589 **< Figure 5 >**

590

4. Conclusions

Based on the experimental (continuous-flow monitoring, batch experiments) and model-based observations presented in this study, we could draw the following conclusions:

- Reactor staging effectively determined a gradient in organic substrate loading and availability in the three-stage pre-denitrifying MBBR. Fluctuations in influent composition led to not negligible dynamics in the denitrification performance during continuous-flow operation, with an overall decrease of denitrification rates after 400 days of operation.
- Retransformation from conjugated metabolites led to the formation of parent sulfonamide antibiotics, namely sulfamethoxazole and sulfadiazine. Possible enantioselective biotransformation was observed for atenolol and citalopram, and a model was developed and successfully calibrated to describe observed removal kinetics.
- As compared to previous findings for nitrifying MBBR and denitrifying activated sludge, enhanced biotransformation kinetics were shown for sulfamethoxazole, erythromycin and atenolol, in particular at higher organic substrate availability. Hence, pre-denitrifying MBBRs operated under increased organic substrate availability may represent a valid option to improve the removal of these three pharmaceuticals.
- Tiered organic substrate loading and quality in single-stage and three-stage MBBRs determined significant differences in the microbial community functions of denitrification and pharmaceutical biotransformation. After more than 450 days of continuous-flow operation, the highest denitrification and pharmaceutical biotransformation kinetics were shown in reactor S1, exposed to the highest electron donor loading and availability.
- When considering all MBBRs, biotransformation rate constants of non-recalcitrant pharmaceuticals positively correlated with mean specific denitrification rates, maximum specific growth rates and catabolic electron fractions. This indicates that biotransformation

615 of pharmaceuticals is likely a cometabolic process, and that microbial activity both in terms
616 of primary (denitrification) and secondary (pharmaceutical biotransformation) metabolic
617 processes activity is more effectively supported by non-limiting organic substrate
618 availability.
619
620 **Acknowledgments**
621 F. Polesel acknowledges financial support from the Technical University of Denmark (DTU),
622 Department of Environmental Engineering for a PhD research fellowship. This research was also
623 supported by MERMAID, ITN funded by the People Programme (Marie Skłodowska-Curie
624 Actions) of the EU FP7/2007-2013/ under REA grant agreement n° 607492', and by the AUFF
625 Center for Advanced Water Purification. The authors are grateful to Carlos Domingo-Félez for
626 scientific discussion and to Mona Refstrup for the support with chemical analyses.
627
628 **References**
629 Alder, A.C., Schaffner, C., Majewsky, M., Klasmeier, J., Fenner, K. (2010). Fate of β-blocker
630 human pharmaceuticals in surface water: Comparison of measured and simulated
631 concentrations in the Glatt Valley Watershed, Switzerland. Water Res. 44, 936–948.
632 Bendz, D., Paxeus, N.A., Ginn, T.R., Loge, F.J. (2005). Occurrence and fate of pharmaceutically
633 active compounds in the environment, a case study: Höje River in Sweden. J. Hazard. Mater.
634 122, 195–204.
635 Beun, J.J., Verhoef, E.V., van Loosdrecht, M.C.M., Heijnen, J.J. (2000). Stoichiometry and
636 kinetics of poly-β-hydroxybutyrate metabolism under denitrifying conditions in activated
637 sludge cultures. Biotechnol. Bioeng. 68, 496–507.
638 Boltz, J.P., Johnson, B.R., Takács, I., Daigger, G.T., Morgenroth, E., Brockmann, D., Kovács,

639 R., Calhoun, J.M., Choubert, J.M., Derlon, N. (2017). Biofilm carrier migration model
640 describes reactor performance. Water Sci. Technol., accepted, doi: 10.2166/wst.2017.160
641 Clesceri, L.S., Greenberg, A.E., Eaton, A.D. (1998). Standard Methods for the Examination of
642 Water and Wastewater (20th edition). APHA, Washington, US.
643 Collado, N., Buttiglieri, G., Ferrando-Climent, L., Rodriguez-Mozaz, S., Barceló, D., Comas, J.,
644 Rodriguez-Roda, I. (2012). Removal of ibuprofen and its transformation products:
645 Experimental and simulation studies. Sci. Total Environ. 433, 296−301.
646 de Graaff, M.S., Vieno, N.M., Kujawa-Roeleveld, K., Zeeman, G., Temmink, H., Buisman,
647 C.J.N. (2011). Fate of hormones and pharmaceuticals during combined anaerobic treatment
648 and nitrogen removal by partial nitritation-anammox in vacuum collected black water. Water
649 Res. 45, 375–383.
650 Ekama, G.A., Wentzel, M.C. (1999). Denitrification kinetics in biological N and P removal
651 activated sludge systems treating municipal wastewaters. Water Sci. Technol. 39, 69–77.
652 Ekama, G.A., Wentzel, M.C. (2008). Nitrogen removal. In Henze, M., van Loosdrecht, M.C.M.,
653 Ekama, G., Brdjanovic, D., "Biological wastewater treatment—principles, modelling and
654 design", IWA Publishing, London, UK.
655 Escher, B.I., Bramaz, N., Richter, M., Lienert, J. (2006). Comparative ecotoxicological hazard
656 assessment of beta-blockers and their human metabolites using a mode-of-action-based test
657 battery and a QSAR approach. Environ. Sci. Technol. 40, 7402–7408.
658 Escolá Casas, M., Chhetri, R.K., Ooi, G., Hansen, K.M.S., Litty, K., Christensson, M.,
659 Kragelund, C., Andersen, H.R., Bester, K. (2015). Biodegradation of pharmaceuticals in
660 hospital wastewater by staged Moving Bed Biofilm Reactors (MBBR). Water Res. 83, 293–
661 302.
662 Evans, S. E., Davies, P., Lubben, A., Kasprzyk-Hordern, B. (2015) Determination of chiral

663 pharmaceuticals and illicit drugs in wastewater and sludge using microwave assisted
664 extraction, solid-phase extraction and chiral liquid chromatography coupled with tandem
665 mass spectrometry. Anal. Chim. Acta 882, 112–126.
666 Falås, P., Baillon-Dhumez, A., Andersen, H.R., Ledin, A., la Cour Jansen, J. (2012). Suspended
667 biofilm carrier and activated sludge removal of acidic pharmaceuticals. Water Res. 46, 1167–
668 1175.
669 Falås, P., Longrée, P., la Cour Jansen, J., Siegrist, H., Hollender, J., Joss, A. (2013).
670 Micropollutant removal by attached and suspended growth in a hybrid biofilm-activated
671 sludge process. Water Res. 47, 4498–4506.
672 Fernandez-Fontaina, E., Omil, F., Lema, J.M., Carballa, M. (2012). Influence of nitrifying
673 conditions on the biodegradation and sorption of emerging micropollutants. Water Res. 46,
674 5434–5444.
675 Ghattas, A.K., Fischer, F., Wick, A., Ternes, T. (2017). Anaerobic biodegradation of (emerging)
676 organic contaminants in the aquatic environment. Water Res., accepted.
677 Göbel, A., Thomsen, A., McArdell, C.S., Joss, A., Giger, W. (2005). Occurrence and sorption
678 behavior of sulfonamides, macrolides, and trimethoprim in activated sludge treatment.
679 Environ. Sci. Technol. 39, 3981–3989.
680 Göbel, A., McArdell, C.S., Joss, A., Siegrist, H., Giger, W. (2007). Fate of sulphonamides,
681 macrolides, and trimethoprim in different wastewater technologies. Sci. Total Environ., 372,
682 361–371.
683 Grady, Jr., C.P.L., Daigger, G.T., Love, N.G., Filipe, C.D.M. (2011). Biological Wastewater
684 Treatment (3rd edition). IWA Publishing, London, UK.
685 Hellauer, K., Mergel, D., Ruhl, A.S., Filter, J., Hübner, U., Jekel, M., Drewes, J.E. (2017).
686 Advancing sequential managed aquifer recharge technology (SMART) using different

687 intermediate oxidation processes. Water 9, 221.
688 Hörsing, M., Ledin, A., Grabic, R., Fick, J., Tysklind, M., la Cour Jansen, J., Andersen, H.R.
689 (2011). Determination of sorption of seventy-five pharmaceuticals in sewage sludge. Water
690 Res. 45, 4470–4482.
691 Jelic, A., Gros, M., Ginebreda, A., Cespedes-Sánchez, R., Ventura, F., Petrovic, M., Barceló, D.
692 (2011). Occurrence, partition and removal of pharmaceuticals in sewage water and sludge
693 during wastewater treatment. Water Res. 45, 1165–1176.
694 Jewell, K.S., Castronovo, S., Wick, A., Falås, P., Joss, A., Ternes, T.A. (2016). New insights
695 into the transformation of trimethoprim during biological wastewater treatment. Water Res.
696 88, 550−557.
697 Joss, A., Zabczynski, S., Göbel, A., Hoffmann, B., Löffler, D., McArdell, C.S., Ternes, T.A.,
698 Thomsen, A., Siegrist, H. (2006). Biological degradation of pharmaceuticals in municipal
699 wastewater treatment: Proposing a classification scheme. Water Res. 40, 1686–1696.
700 Kasprzyk-Hordern, B., Baker, D.R. (2011). Enantiomeric profiling of chiral drugs in wastewater
701 and receiving waters. Environ. Sci. Technol. 46, 1681–1691.
702 Kujawa, K., Klapwijk, B. (1999) A method to estimate denitrification potential for
703 predenitrification systems using NUR batch test. Water Res. 33, 2291–2300.
704 Lee, H.J., Lee, E., Yoon, S.H., Chang H.R., Kim, K., Kwon, J.H. (2012). Enzymatic and
705 microbial transformation assays for the evaluation of the environmental fate of diclofenac and
706 its metabolites. Chemosphere 87, 969–974.
707 MacLeod, S.L., Sudhir, P., Wong, C.S. (2007). Stereoisomer analysis of wastewater-derived β-
708 blockers, selective serotonin re-uptake inhibitors, and salbutamol by high-performance liquid
709 chromatography–tandem mass spectrometry. J. Chromatogr. A 1170, 23–33.
710 Maurer, M., Escher, B.I., Richle, P., Schaffner, C., Alder, A.C. (2007). Elimination of β-blockers

711 in sewage treatment plants. Water Res. 41, 1614–1622.
712 Muller, A., Wentzel, M.C., Loewenthal, R.E., Ekama, G.A. (2003). Heterotroph anoxic yield in
713 anoxic aerobic activated sludge systems treating municipal wastewater. Water Res. 37, 2435–
714 2441.
715 Nikolai, L.N., McClure, E.L., MacLeod, S.L., Wong, C.S. (2006). Stereoisomer quantification
716 of the β-blocker drugs atenolol, metoprolol, and propranolol in wastewaters by chiral high-
717 performance liquid chromatography–tandem mass spectrometry. J. Chromatogr. A 1131,
718 103–109.
719 Ødegaard, H., Rusten, B., Westrum, T. (1994). A new moving bed bofilm reactor—Applications
720 and results. Water Sci. Tech., 29, 157–165.
721 Pan, Y., Ni, B.J., Lu, H., Chandran, K., Richardson, D., Yuan, Z. (2015). Evaluating two
722 concepts for the modelling of intermediates accumulation during biological denitrification in
723 wastewater treatment. Water Res. 71, 21–31.
724 Plósz, B.G. (2007). Optimization of the activated sludge anoxic reactor configuration as a means
725 to control nutrient removal kinetically. Water Res. 41, 1763–1773.
726 Plósz, B.G., Vogelsang, C., Macrae, K., Heiaas, H.H., Lopez, A., Liltved, H., Langford, K.H.
727 (2010a). The BIOZO process – a biofilm system combined with ozonation: occurrence of
728 xenobiotic organic micro-pollutants in and removal of polycyclic aromatic hydrocarbons and
729 nitrogen from landfill leachate. Water Sci. Technol. 61, 3188–3197.
730 Plósz, B.G., Leknes, H., Thomas, K.V. (2010b). Impacts of competitive inhibition, parent
731 compound formation and partitioning behaviour on antibiotic micro-pollutants removal in
732 activated sludge. Environ. Sci. Technol., 44, 734–742.
733 Plósz, B.G., Langford, K.H., Thomas, K.V. (2012). An activated sludge model for trace
734 xenobiotic chemicals (ASM-X): Assessment of diclofenac and carbamazepine. Biotechnol.

735 Bioeng., 109, 2757–2769.
736 Plósz, B.G., Reid, M.J, Borup, M., Langford, K.H., Thomas, K.V. (2013). Biotransformation
737 kinetics and sorption of cocaine and its metabolites and the factors influencing their
738 estimation in wastewater. Water Res., 47, 2129–2140.
739 Polesel, F., Andersen, H.R., Trapp, S., Plósz, B.G. (2016). Removal of antibiotics in biological
740 wastewater treatment systems—A critical assessment using the Activated Sludge Modeling
741 Framework for Xenobiotics (ASM-X). Environ. Sci. Technol. 50, 10316–10334.
742 Radjenovic, J., Petrovic, M., Barceló, D. (2009). Fate and distribution of pharmaceuticals in
743 wastewater and sewage sludge of the conventional activated sludge (CAS) and advanced
744 membrane bioreactor (MBR) treatment. Water Res. 43, 831–841.
745 Radke, M., Lauwigi, C., Heinkele, G., Mürdter, T.E., Letzel, M. (2009). Fate of the antibiotic
746 sulfamethoxazole and its two major human metabolites in a water sediment test. Environ. Sci.
747 Technol. 43, 3135–3141.
748 Reichert, P. (1998). AQUASIM 2.0—Computer Program for the Identification and Simulation
749 of Aquatic Systems. EAWAG, Dübendorf, Switzerland.
750 Ribeiro, A.R., Afonso, C.M., Castro, P.M.L., Tiritan, M.E. (2013). Enantioselective HPLC
751 analysis and biodegradation of atenolol, metoprolol and fluoxetine. Environ. Chem. Lett. 11,
752 83–90.
753 Roeleveld, P.J., van Loosdrecht, M.C.M. (2002). Experience with guidelines for wastewater
754 characterisation in The Netherlands. Water Sci. Technol. 45, 77–87.
755 Sathyamoorthy, S., Chandran, K., Ramsburg, C.A. (2013). Biodegradation and cometabolic
756 modeling of selected beta blockers during ammonia oxidation. Environ. Sci. Technol. 47,
757 12835−12843.
758 Scuras, S.E., Jobbágy, A., Grady, Jr., C.P.L. (2001). Optimization of activated sludge reactor

759 configuration: kinetic considerations. Water Res. 35, 4277–4284.
760 Stadler, L.B., Su, L., Moline, C.J., Ernstoff, A.S., Aga, D.S., Love, N.G. (2015). Effect of redox
761 conditions on pharmaceutical loss during biological wastewater treatment using sequencing
762 batch reactors. J. Hazard. Mater. 282, 106–115.
763 Stierlin, H., Faigle, J.W. (1979). Biotransformation of diclofenac sodium (Voltaren®) in animals
764 and in man.: II. Quantitative determination of the unchanged drug and principal phenolic
765 metabolites, in urine and bile. Xenob. 9, 611–621.
766 Su, L., Aga, D., Chandran, K., Khunjar, W.O. (2015). Factors impacting biotransformation
767 kinetics of trace organic compounds in lab-scale activated sludge systems performing
768 nitrification and denitrification. J. Hazard. Mater. 281, 116–124.
769 Suarez, S., Lema, J.M., Omil, F. (2010). Removal of Pharmaceutical and Personal Care Products
770 (PPCPs) under nitrifying and denitrifying conditions. Water Res. 44, 3214–3224.
771 Tan, D.T., Arnold, W.A., Novak, P.J. (2013). Impact of organic carbon on the biodegradation of
772 estrone in mixed culture systems. Environ. Sci. Technol. 47, 12359−12365.
773 Ternes, T.A., Herrmann, N., Bonerz, M., Knacker, T., Siegrist, H., Joss, A. (2004). A rapid
774 method to measure the solid–water distribution coefficient (K_d) for pharmaceuticals and musk
775 fragrances in sewage sludge. Water Res. 38, 4075–4084.
776 Torresi, E., Fowler, S.J., Polesel, F., Bester, K., Andersen, H.R., Smets, B.F., Plósz, B.G.,
777 Christensson, M. (2016). Biofilm thickness influences biodiversity in nitrifying MBBRs –
778 Implications on micropollutant removal. Environ. Sci. Technol. 50, 9279–9288.
779 Torresi, E., Escolá Casas, M., Polesel, F., Plósz, B.G., Christensson, M., Bester, K. (2017).
780 Impact of external carbon dose on the removal of micropollutants using methanol and ethanol
781 in post-denitrifying Moving Bed Biofilm Reactors. Water Res. 108, 95–105.
782 Torresi, E. (2017). Removal of micropollutants in Moving Bed Biofilm reactors (MBBRs) —

783 Microbial structure and function relationships. PhD dissertation, DTU Environment,
784 Technical University of Denmark.
785 Ubay Çokgör, E., Sözen, S., Orhon, D., Henze, M. (1998). Respirometric analysis of activated
786 sludge behaviour—I. Assessment of the readily biodegradable substrate. Water Res. 32, 461–
787 475.
788 van der Ven, A.J.A.M., Vree, T.B., van Ewijk-Beneken Kolmer, E.W.J., Koopmans, P.P., van
789 der Meer, J.W.M. (1995). Urinary recovery and kinetics of sulphamethoxazole and its
790 metabolites in HIV-seropositive patients and healthy volunteers after a single oral dose of
791 sulphamethoxazole. Br. J. Clin. Pharmac. 39, 621–625.
792 Vazquez-Roig, P., Kasprzyk-Hordern, B., Blasco, C., Picó, Y. (2014). Stereoisomeric profiling
793 of drugs of abuse and pharmaceuticals in wastewaters of Valencia (Spain). Sci. Total Environ.
794 494–495, 49–57.
795 Vieno, N., Sillanpää, M. (2014). Fate of diclofenac in municipal wastewater treatment–A review.
796 Environ. Intern. 69, 28–39.
797 Vree, T.B., Hekster, Y.A. (1987). Clinical pharmacokinetics of sulfonamides and their
798 metabolites – An encyclopedia. Antibiot. Chemother. 37, 1–214.
799 Vree T.B., van der Ven, A.J.A.M., Koopmans, P.P., van Ewijk-Beneken Kolmer, E.W.J.,
800 Verwey-van Wissen, C.P.W.G.M. (1995). Pharmacokinetics of sulfamethoxazole with its
801 hydroxy metabolites and N4-acetyl-, N1-glucuronide conjugates in healthy human volunteers.
802 Clin. Drug Invest. 9, 43–53.
803 Weiss, S., Reemtsma, T. (2008). Membrane bioreactors for municipal wastewater treatment – A
804 viable option to reduce the amount of polar pollutants discharged into surface waters? Water
805 Res. 42, 3837–3847.
806 Wick, A., Fink, G., Joss, A., Siegrist, H., Ternes, T.A. (2009). Fate of beta blockers and psycho-

active drugs in conventional wastewater treatment. Water Res. 43, 1060–1074.

Zhang, Y., Geißen, S.U., Gal, C. (2008). Carbamazepine and diclofenac: Removal in wastewater treatment plants and occurrence in water bodies. Chemosphere 73, 1151–1161.

811 **Tables**

812 **Table 1.** Summary of model structures identified and used in this study to describe
813 pharmaceutical concentration profiles observed during batch experiments (batch 1 and 2).

Case	Processes	State variables				Rate equation
		C_{LI}	$C_{EN,1}$	$C_{EN,2}$	C_{CJ}	
Biotransformation only (Fig. 3a)	Biotransformation of C_{LI}	-1				$\frac{k_{bio}}{1+K_d X_{SS}} C_{LI} X_{SS}$
Biotransformation and retransformation (Fig. 3b–c)	Biotransformation of C_{LI}	-1				$\frac{k_{bio}}{1+K_d X_{SS}} C_{LI} X_{SS}$
	Formation of C_{LI}	+1 (+F)*			-1	$k_{dec} C_{CJ} X_{SS}$
Enantioselective biotransformation (Fig. 3d)	Biotransformation of enantiomer 1	(-1)	-1			$\frac{k_{bio,1}}{1+K_d X_{SS}} C_{EN,1} X_{SS}$
	Biotransformation of enantiomer 2	(-1)		-1		$\frac{k_{bio,2}}{1+K_d X_{SS}} C_{EN,2} X_{SS}$

*In case the pharmaceutical has only one known retransformable conjugate (SDZ and AcSDZ), the stoichiometry coefficient F should be used, being equivalent to the ratio of the molecular weight of parent (M_{LI}) and conjugated (M_{CJ}) pharmaceutical.

814

Table 2. Summary of kinetic (k_{bio}, k_{dec}, $k_{bio,1}$, $k_{bio,2}$ in L gTSS^{-1} d^{-1}) and stoichiometric (*EF*—including the two respective fraction of enantiomer 1 and 2—and $n_{LI,CJ}$) parameters estimated in this study on pharmaceutical biotransformation and comparison with literature values.

Chemical	Parameter	Batch 1	Batch 2	Literature	Ref[4]	Conditions[5]
ATN[1,3]	$k_{bio,1}$	2.7–4.3				
	$k_{bio,2}$	0.0				
	EF	0.19 (0.81)		0.30–0.53	*A–E*	RI
	k_{bio}		1.1–2.4	0.7–0.8	*F*	DNAS
				0.5–5.0	*F, G, H*	NMBBR
				5.1–6.4	*I*	DNMBBR
CIT[3]	$k_{bio,1}$		2.9–5.1			
	$k_{bio,2}$		0.0–0.4			
	k_{bio}			0.7–3.1	*H*	NMBBR
				2.9–4.3	*I*	DNMBBR
	EF		0.52 (0.48)	0.56–0.60	*B, E*	RI
ERY[1]	k_{bio}		0.3–1.0	0.2	*J*	DNAS
				0.2–0.9	*G, H*	NMBBR
				0.2–0.6	*I*	DNMBBR
IBU[1]	k_{bio}		0.00–0.03	1.5	*J*	DNAS
				0–31	*H, K*	NMBBR
				0.5–1.4	*I*	DNMBBR
IOH[1]	k_{bio}		0.00–0.03	0.0–2.2	*G, H*	NMBBR
				0.3–0.7	*I*	DNMBBR
SMZ[1]	k_{bio}		0.02–0.09	0.2–0.9	*G, H*	NMBBR
				0.0–3.3	*I*	DNMBBR
TMP[1]	k_{bio}	0.4–1.0	0.1–0.3	≤0.1–1.3	*F, L*	DNAS
				0.1–3.3	*F, G, H*	NMBBR
				2.1–4.1	*I*	DNMBBR
VFX[1]	k_{bio}		0.02–0.06	≤0.1	*F*	DNAS
				≤0.1–0.3	*F, G, H*	NMBBR
				0.1–1.9	*I*	DNMBBR
DCF[2]	k_{bio}	0.0	0.00–0.05	<0.1–1.0	*F, J, M*	DNAS
				0.1–5.8	*F, G, H, K*	NMBBR
				0.0	*I*	DNMBBR
	k_{dec}	3.7–7.4		5.0	*M*	DNAS
				1.6–2.5	*G*	NMBBR
	$n_{LI,CJ}$	4.50		0.85	*M*	SI
MET[2]	k_{bio}	0.1–0.3	0.0	≤0.1	*F*	DNAS
				0.3–1.2	*F, G, H*	NMBBR
				0.4–0.8	*I*	DNMBBR
	k_{dec}	0.5–2.4				
	$n_{LI,CJ}$	3.80				

SMX[2]	k_{bio}	0.7–2.2	1.0–3.5	0.4	*N*	DNAS
				0.2–1.0	*G, H*	NMBBR
				0.1–3.2	*I*	DMBBR
	k_{dec}	1.9–6.5	0.5–2.1	1.1–7.9	*F, N*	DNAS
				0.7–1.6	*F*	NMBBR
	$n_{LI,CJ}$	0.73	0.15	0.13–0.66	*N, O*	SI
SDZ[2] (Ac-SDZ)	k_{bio}	0.7–1.7		0.1–0.7	*G, H*	NMBBR
				0.6–1.0	*I*	DNMBBR
	k_{dec}	1.0–2.0		<0.1–8.4	*G, H*	NMBBR
				3.7–4.2	*I*	DNMBBR

[1]Biotransformation only (Eq. 3); [2]Bio- and retransformation (Eqs. 4–6); [3]Enantioselective biotransformation (Eq. 9–10); [4]References: A=Nikolai et al. (2006); B=MacLeod et al. (2007); C=Kasprzyk-Hordern and Baker (2011); D=Vazquez-Roig et al. (2014); E=Evans et al. (2015); F=Falås et al. (2013) (rate constants as L $gTAS^{-1}$ d^{-1}); G=Torresi et al. (2016) (rate constants as L gTAS d^{-1}); H=Escolá-Casas et al. (2015) (rate constants as L gTAS d^{-1}); I=Torresi et al. (2017) (rate constants as L gTAS d^{-1}); J=Suarez et al. (2010) (rate constants as L $gVSS^{-1}$ d^{-1}); K=Falås et al. (2012) (rate constants as L $gTAS^{-1}$ d^{-1}); L=Su et al. (2015) (rate constants as L $gCOD^{-1}$ d^{-1}); M=Plósz et al. (2012) (rate constants as L $gTSS^{-1}$ d^{-1}); N=Plósz et al. (2010b) (rate constants as L $gTSS^{-1}$ d^{-1}); O=Göbel et al. (2007); [5]Abbreviations: DNAS=Denitrifying Activated Sludge; NMBBR=Nitrifying MBBR; DNMBBR=Denitrifying MBBR; RI=Raw Influent; SI=Secondary Influent.

Figures

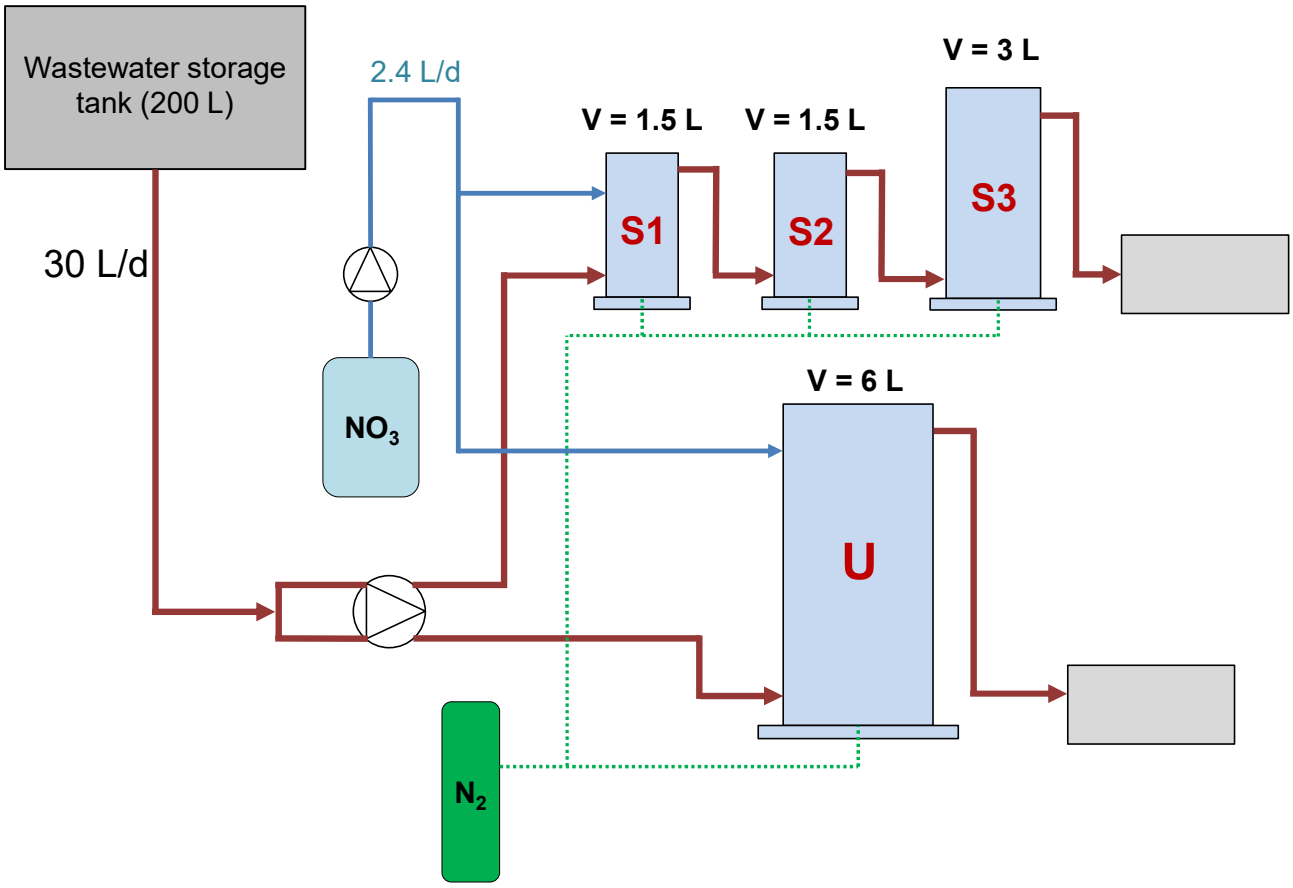

Figure 1. Schematic representation of three-stage (S1, S2, S3) and single-stage (U) MBBR systems under continuous-flow operation. The two MBBRs, having overall the same filling ratio (33%) and working volume (6 L), were operated in parallel with the same influent flow rate (16.2 L d^{-1}) and thus the same hydraulic residence time (HRT=8.9 h). External dosing of potassium nitrate (KNO_3) was performed to achieve an influent NO_3-N concentration of 103 mgN L^{-1} in S1 and U reactors. Sparging of N_2 gas was used in each MBBR to minimize oxygen penetration and ensure carrier mixing in the reactors.

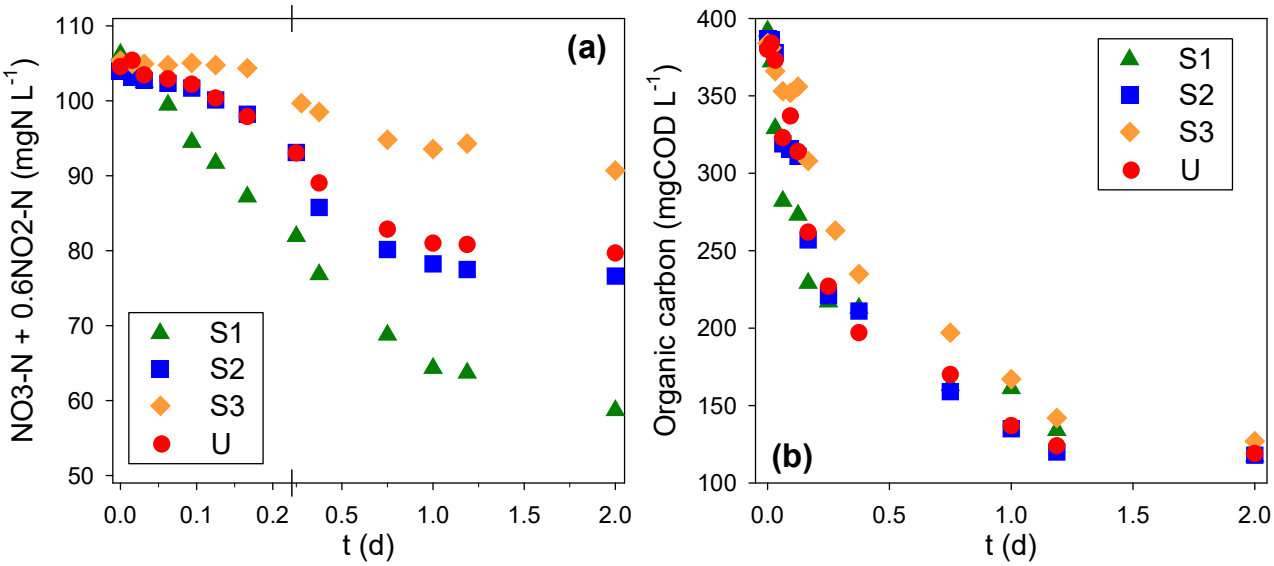

Figure 2. Concentration profiles of NO_X (a) and total COD (b) measured during anoxic respirometry (batch 2) in different MBBR reactors. The x-axis in (a) is intentionally subdivided in two parts of different scales to highlight lag phases in NO_X reduction in S2, U and S3.

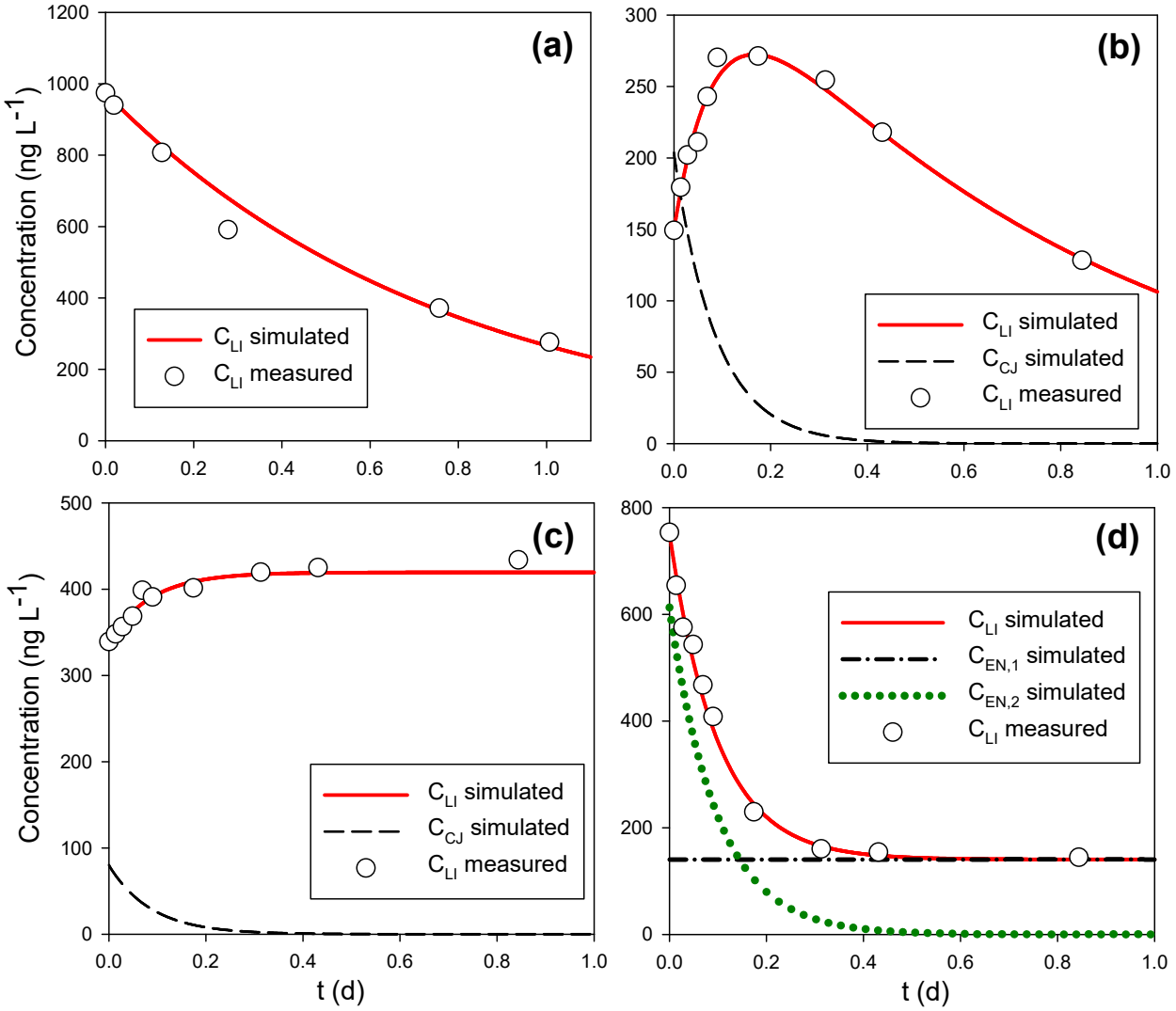

Figure 3. Typical profiles of pharmaceutical concentrations observed during batch experiments (circles) and simulation results with calibrated model (full, dashed and dotted lines): (a) biotransformation only (ATN, batch 2; Eq. 3); (b, c) retransformation and biotransformation (b: SMX, batch 1; c: DCF, batch 1; Eq. 5–6); (d) enantioselective biotransformation (ATN, batch 1; Eq. 9).

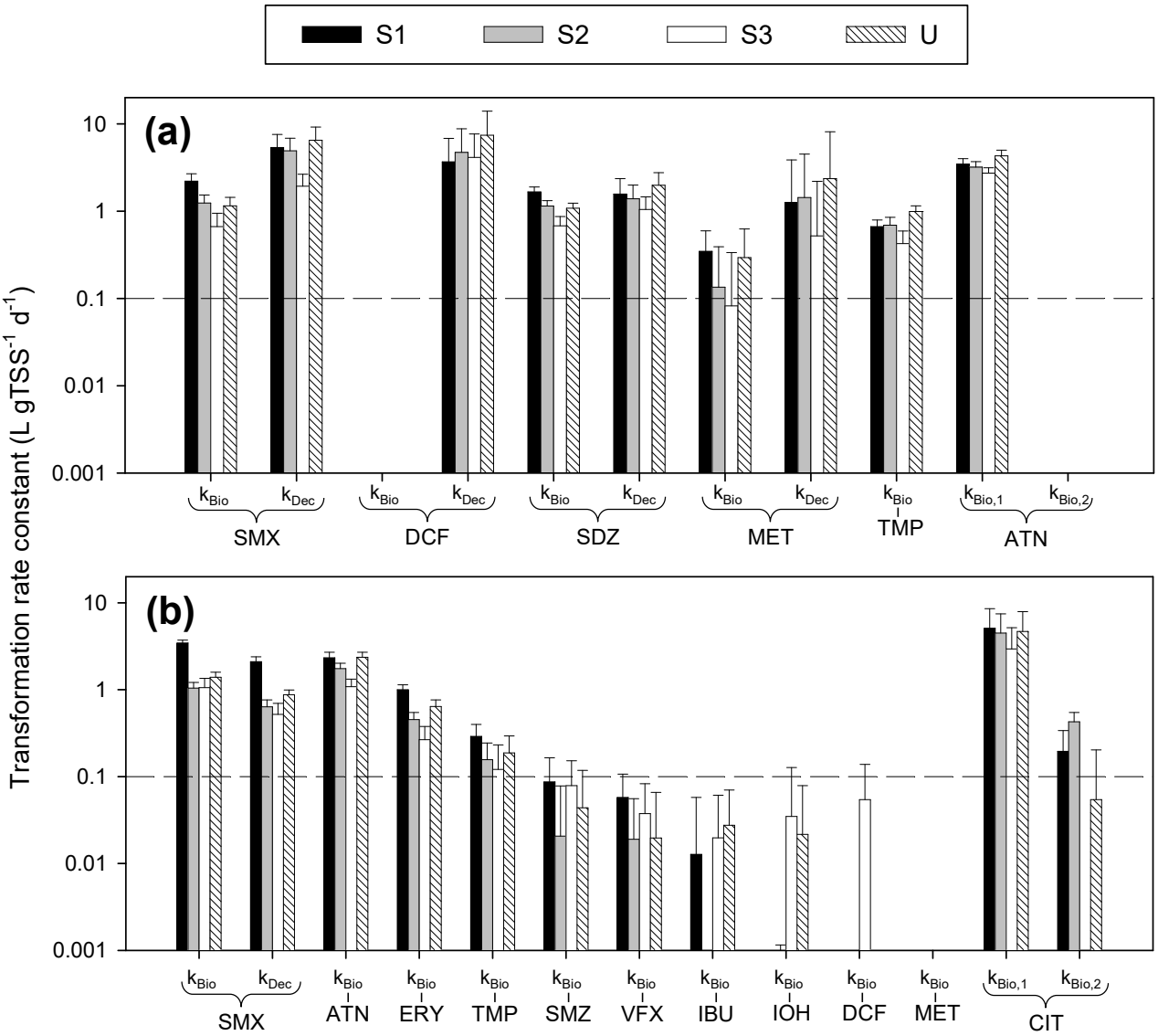

Figure 4. Estimated transformation rate constants for pharmaceuticals in batch 1 (a) and batch 2 (b). The dashed line at k_{bio} = 0.1 L $gTSS^{-1}$ d^{-1} (Joss et al., 2006) is used as threshold to identify recalcitrant and non-recalcitrant pharmaceuticals.

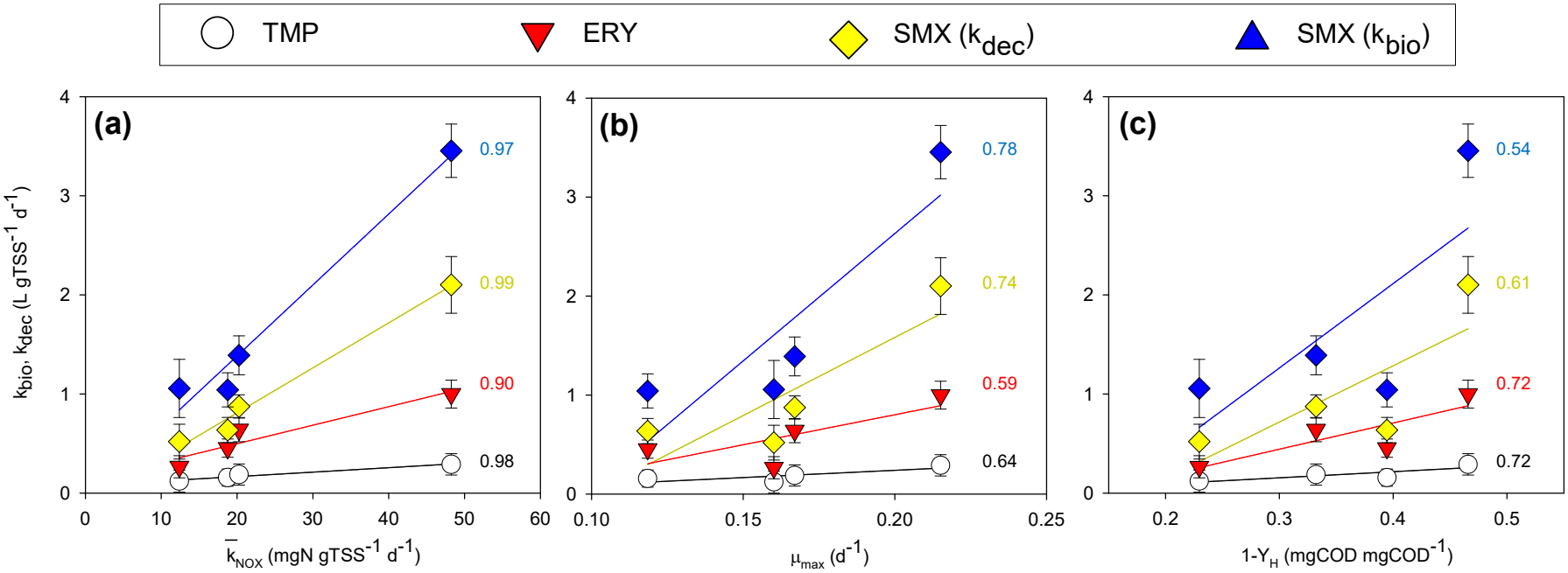

Figure 5. Estimated transformation rate constants (k_{bio}, k_{dec}) for non-recalcitrant pharmaceuticals plotted as a function of (a) mean specific denitrification rate ($\bar{k}_{NOX}$), (b) maximum specific growth rate (μ_{max}) and (c) catabolic electron fraction (1-Y_H) during batch 2 in different MBBR reactors (S1, S2, S3, U). Linear regressions (solid lines) are used to indicate the possible correlation between denitrification and pharmaceutical removal kinetics for each substance (numbers in the figure denote the R^2 values of each regression).